Nanoscale

Cite this: *Nanoscale*, 2012, **4**, 4674

www.rsc.org/nanoscale

PAPER

Biosensor based on Prussian blue nanocubes/reduced graphene oxide nanocomposite for detection of organophosphorus pesticides

Lin Zhang,[a] Aidong Zhang,[a] Dan Du*[a] and Yuehe Lin*[b]

Received 23rd April 2012, Accepted 31st May 2012
DOI: 10.1039/c2nr30976a

We demonstrate a facile procedure to efficiently prepare Prussian blue nanocubes/reduced graphene oxide (PBNCs/rGO) nanocomposite by directly mixing Fe^{3+} and $[Fe(CN)_6]^{3-}$ in the presence of GO in polyethyleneimine aqueous solution, resulting in a novel acetylcholinesterase (AChE) biosensor for detection of organophosphorus pesticides (OPs). The obtained nanocomposite was characterized by X-ray photoelectron spectroscopy (XPS), transmission electron microscopy (TEM) and energy-dispersive X-ray (EDX) microanalysis. It was clearly observed that the nanosheet has been decorated with cubic PB nanoparticles and nearly all the nanoparticles are distributed uniformly only on the surface of the reduced GO. No isolated PB nanoparticles were observed, indicating the strong interaction between PB nanocubes and the reduced GO and the formation of PBNCs/rGO nanocomposite. The obtained PBNCs/rGO based AChE biosensor make the peak potential shift negatively to 220 mV. The over-potential decreases ~460 mV compared to that on a bare electrode, suggesting that PBNCs/rGO has a high electrocatalytic activity towards the oxidation of thiocholine. The AChE biosensor shows rapid response and high sensitivity for detection of monocrotophos with a linear range from 1.0 to 600 ng mL^{-1} and a detection limit of 0.1 ng mL^{-1}. These results suggest that the PBNCs/rGO hybrids nanocomposite exhibited high electrocatalytic activity towards the oxidation of thiocholine, which lead to the sensitive detection of OP pesticides.

Introduction

Because of the high toxicity of organophosphorus pesticides (OPs), they still remain a serious health threat to humans across the world. Rapid detection of these toxic agents has become increasingly important for health protection.[1,2] Although gas or liquid chromatography and mass spectrometry are accurate and routinely performed for analyzing OPs,[3,4] these methods have a number of disadvantages, limiting their applications for rapid analyses under field conditions. Development of a simple, rapid, sensitive and inexpensive method with real-time output to detect OPs is of considerable interest.

Enzyme-based biosensors have emerged in the past few years as the most promising alternative technique for on-site detection of pesticides.[5–7] Various inhibition and non-inhibition biosensor systems, based on the immobilization of acetylcholinesterase (AChE) or OP hydrolase (OPH) have been developed. The key step for enhancing the sensitivity of the biosensors is to improve the biosensor design and the electrochemical detection of the enzymatic product. In order to reduce the oxidation potential of enzymatic product thiocholine on conventional electrodes,[8,9] mediators such as cobalt(II) phthalocyanine[10,11] and Prussian blue[12,13] have been used. The ideal biosensor should provide a large surface area for large quantities of enzymes to be immobilized and provide a favorable microenvironment to maintain the enzyme activity.

The recent discovery of graphene in 2004 (ref. 14) has attracted much attention for its two-dimensional structure and novel physical properties and potential applications in nanoelectronic devices and transparent conductors.[15–18] It is an ideal material for electrochemistry because of the large surface area, excellent electrical conductivity and low cost.[19] More recently, different kinds of metal nanoparticles have been introduced into graphene, such as Au,[20,21] TiO_2,[22,23] SnO_2 (ref. 24) to strengthen the activity. Graphene-based nanocomposites have been developed as an enhanced sensing platform for biosensors, because these kinds of nanocomposite films may generate synergistic effect to enhance the sensitivity. However, it is difficult to synthesize graphene sheet-based nanocomposites using exfoliated graphene sheet directly because of their limited solubility in solution.[25] Graphene oxide (GO), achieved in large scale by exfoliating graphite oxide with the assistance of ultrasound radiation, has as large a surface area as graphene and possesses large numbers of oxygen-containing functional groups, such as hydroxyl, carboxyl and epoxy groups,[26–28] offering us a

[a]*Key Laboratory of Pesticide and Chemical Biology of Ministry of Education, College of Chemistry, Central China Normal University, Wuhan 430079, PR China. E-mail: dudan@mail.ccnu.edu.cn; Fax: +86 27 67867953; Tel: +86 27 67867958*
[b]*Pacific Northwest National Laboratory, Richland, WA 99352, USA. E-mail: yuehe.lin@pnnl.gov; Fax: +1 509 371 6241; Tel: +1 509 371 6241*

potential precursor for such nanocomposite fabrication. For example, GO–silica,[29] GO–sulfonated polyaniline[30] and GO–metal nanocomposites[31,32] were synthesized and further converted to graphene sheet-based nanocomposites by chemical deoxygenation. Moreover, GO can also improve the properties of nanoparticles on their surface.[33] Chen reported an ultrafine Pd nanoparticles–GO nanocomposite surface which expresses higher activity in formic acid and ethanol oxidation compared with a commercial Pd/C catalyst.[34] Moreover, PB nanocomposites decorated on graphene[35] or graphene oxide[36] has been reported, with excellent electrocatalytic activity towards H_2O_2.

In this paper, we demonstrate a facile procedure to efficiently prepare Prussian blue nanocubes/reduced graphene oxide (PBNCs/rGO) nanocomposites by directly mixing Fe^{3+} and $(Fe(CN)_6)^{3-}$ in the presence of GO in polyethyleneimine aqueous solution. The PBNCs/rGO nanocomposite was used for fabrication of an AChE biosensor by directly coating an AChE layer over the nanocomposite film on the electrode surface (Scheme 1). Prussian blue (PB) differs favourably from many other modifiers applied in enzyme sensors by its high efficiency of electron transfer in a wide pH range, by the stability of its electrochemical characteristics and the simple procedures for deposition and activation.[37] It was found that the obtained PBNCs/rGO hybrids nanocomposite modified electrode exhibited high electrocatalytic activity towards the oxidation of thiocholine, a hydrolysis product of the AChE substrate, which prevented the potential interference from other electroactive species.

Experimental

1. Reagents

Monocrotophos was purchased from Dr Ehrenstorfer GmbH (Augsburg, Germany). Human AChE, acetylthiocholine chloride (ATCl), pralidoxime iodide, chitosan and phosphate buffered saline were purchased from Sigma-Aldrich Co. (St. Louis, USA). Polyethyleneimine (PEI) was obtained from Aladdin Chemistry Co. (Shanghai, China). Graphite powder, potassium ferricyanide ($K_3Fe(CN)_6$), potassium chloride (KCl), ferric chloride ($FeCl_3 \cdot 6H_2O$), hydrochloric acid (HCl), sulfuric acid (H_2SO_4), potassium permanganate ($KMnO_4$) and hydrogen peroxide solution (H_2O_2, 30 wt%) were obtained from Shanghai Chemical Reagent Co. (Shanghai, China).

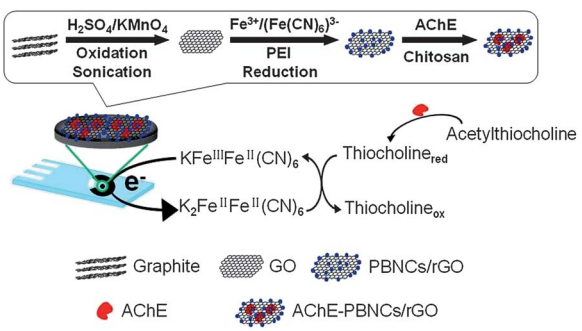

Scheme 1 Preparation of PBNCs/rGO nanocomposite-based AChE biosensor and the electrocatalytic mechanism for ATCl oxidation.

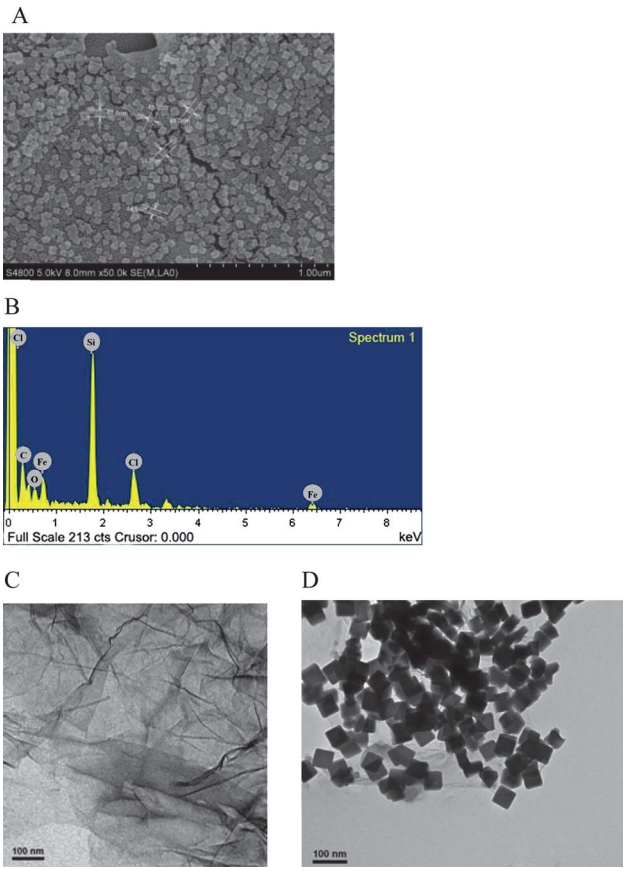

Fig. 1 (A) SEM image and (B) EDX pattern of PBNCs/rGO nanocomposite. (C) TEM image of GO and (D) TEM of PBNCs/rGO nanocomposite.

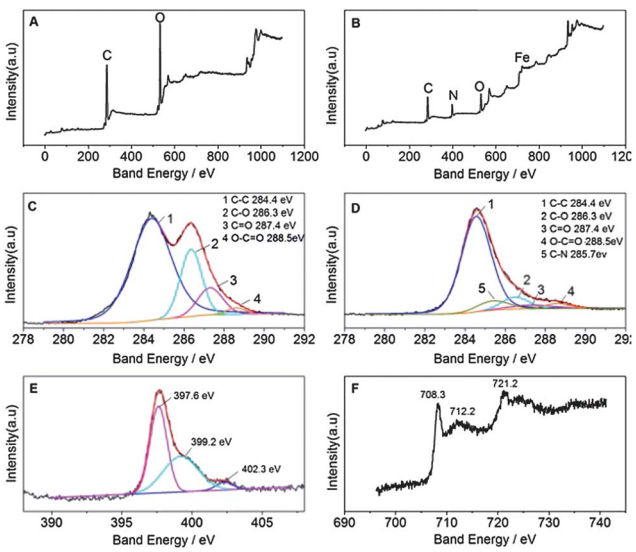

Fig. 2 (A) XPS spectra of GO, (B) PBNCs/rGO nanocomposite, (C) C1s of GO, (D) C1s of PBNCs/rGO nanocomposite, (E) N1s of PBNCs/rGO nanocomposite and (F) Fe2p of PBNCs/rGO nanocomposite.

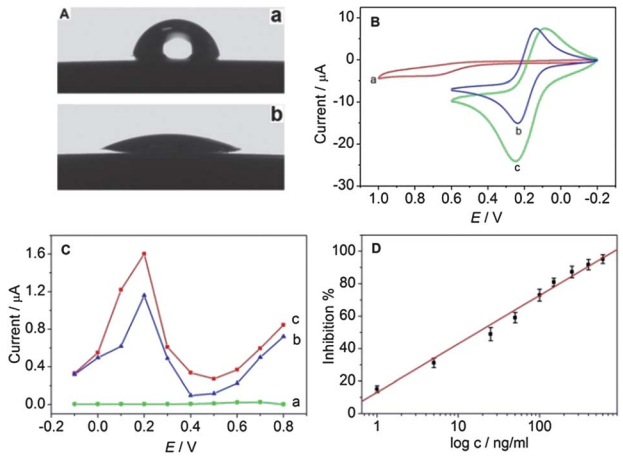

Fig. 3 (A) Contact angle graphs of bare electrode (a) and PBNCs/rGO nanocomposite modified electrode (b). (B) Cyclic voltammograms of bare SPE in PBS (a); AChE–PBNCs/rGO/SPE in PBS in the absence of ATCl (b) and AChE–PBNCs/rGO/SPE in PBS in the presence of ATCl (c). (C) Hydrodynamic voltammograms obtained at AChE/SPE (a); AChE–PB/SPE (b) and AChE–PBNCs/rGO/SPE (c) in PBS containing 3.0 mM ATCl. (D) Calibration curve of the inhibition percentage and different concentrations of monocrotophos.

Table 1 Current-time response of AChE biosensor in PBS

	Current/μA	Response time/s
AChE/SPE	1.4	26
AChE–PB/SPE	10.7	20.6
AChE–PBNCs/rGO/SPE	15.2	10.9

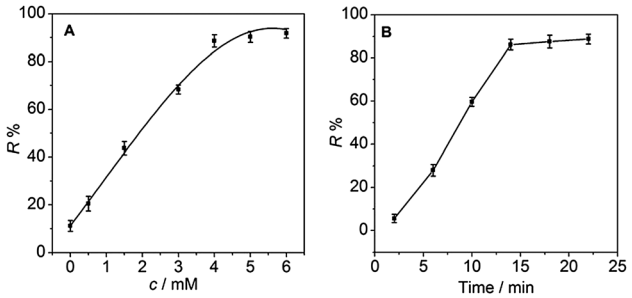

Fig. 4 Effects of incubation concentration (A) and incubation time (B) of pralidoxime iodide on reactivation efficiency.

Table 2 Recovery studies of monocrotophos in cucumber samples

Sample no.	Amount spiked/ng mL^{-1}	Found/ng mL^{-1}	Recovery(%)
1	5	5.13	102.6
2	10	9.91	99.1
3	100	102.5	102.5
4	300	309.8	103.3
5	500	488.7	97.7

2. Synthesis of graphene oxide (GO)

The preoxidized graphite was reoxidized by the Hummer's method. Briefly, 0.5 g pretreated graphite was put into 20 mL cold concentrated H_2SO_4 (0 °C). Then, 1.5 g $KMnO_4$ was added gradually under stirring with the system temperature below 20 °C by an ice bath. The mixture was then stirred at 35 °C for 2 h, followed by the addition of distilled water (50 mL), and stirring was continued for 15 min. To complete the reaction, distilled water (140 mL) was then added to the mixture. Subsequently, 30% H_2O_2 (2 mL) was added drop-by-drop and the color of the mixture changed to bright yellow. The mixture was filtered and washed with an aqueous HCl solution (v/v 1 : 10) (250 mL) to remove metal ions, followed by a wash with distilled water to remove the acid until the solution became neutral. Exfoliation was carried out by sonicating the GO dispersion (0.5 mg mL^{-1}) for 1 h.

3. Synthesis of Prussian blue nanocubes/reduced graphene oxide (PBNCs/rGO) nanocomposite

The PBNCs/rGO nanocomposite was synthesized similarly to a reported method.[38] Briefly, 10 mL $K_3Fe(CN)_6$ (5 mM, pH 1.1), 1.0 mL of 3% PEI, and 10 mL $FeCl_3 \cdot 6H_2O$ (5 mM, pH 1.1) were added to 10 mL of GO dispersion (0.5 mg mL^{-1}, pH 1.1) under stirring, and the mixture was heated and refluxed for 3 h. The colour of the mixture gradually changed from yellow to dark cyan, indicating the successful preparation of PBNCs/rGO nanocomposite. The obtained product was washed with distilled water three times and collected by centrifugation.

4. Characterization

Scanning electron microscopy (SEM) and energy-dispersive X-ray (EDX) microanalysis were performed by using an S-4800 field-emission scanning electron microscope (HITACHI, Japan). SEM-EDX analyzes were performed on the surface of silica and at least five analyses at different spots were performed for each sample to obtain an average value. Transmission electron microscopy (TEM) images were obtained with JEM 1230 transmission electron microscope (JEOL, Japan) operated at 160 KV. The static water contact angle of PBNCs/rGO was measured at 25 °C by a contact angle system OCA 20 (Data-physics, Germany). X-Ray photoelectron spectroscopy (XPS) measurements were carried out with a thermoelectron instrument MultiLab 2000 (Thermo Fisher, USA). Electrochemical characterization was carried out with a CHI 660C Electrochemical Workstation (Shanghai Chenhua Instrument Co., China). Before electrochemical measurement, 3.0 μL of the above PBNCs/rGO nanocomposite was first coated on a pretreated screen printed electrode (SPE). After drying for 1 h, 5.0 μL AChE chitosan (0.05%) solution was introduced onto the PBNCs/rGO nanocomposite modified electrode to obtain an AChE biosensor. Monocrotophos was used as a model OP compound for this study. The inhibition efficiency (I%) was calculated as: $I\% = 100\% \times (i_0 - i)/i_0$, where i_0 and i are the peak currents of ATCl before and after monocrotophos inhibition. The inhibited AChE modified electrode was reactivated with 5.0 mM pralidoxime iodide for 15 min, then added 50 μL 3.0 mM ATCl in PBS to study the electrochemical response.

The reactivation efficiency (R%) was estimated as: $R(\%) = 100\% \times (i_r - i)/(i_0 - i)$, where i_r was the peak current of ATCl with pralidoxime iodide reactivation. Square-wave voltammetric (SWV) measurement was used for detection with the potential range from −0.2 to 0.8 V at 50 mV s^{-1} scanning rate.

Results and discussion

The typical morphology of a PBNCs/rGO nanocomposite is shown in an SEM image (Fig. 1A), which exhibits a large quantity of cubic nanoparticles with average size of ~50 nm. The EDX measurements further confirm the high content of iron and carbon in the nanocomposites. A typical spectrum is presented in Fig. 1B, where peaks associated with Fe, Si, C, O and Cl can be distinguished. The oxygen and silicon are presumably due to the thickness of the silicon oxide layer. The large amount of chlorine is assigned to the electrolyte of KCl remaining in the synthesis.

In addition, overall morphological information on the reduced GO and PBNCs/rGO nanocomposites were provided by the TEM images. The reduced GO displayed a silk-like structure with single or very thin layers (Fig. 1C). It is observed that the nanosheet has been decorated with cubic PB nanoparticles and nearly all the nanoparticles are distributed uniformly only on the surface of the reduced GO (Fig. 1D). The TEM images further reveal that there is no observation of isolated PB nanoparticles, indicating the strong interaction between PB nanocubes and the reduced GO, and the formation of a PBNCs/rGO nanocomposite.

Details of the chemical changes during *in situ* reduction of GO for the preparation of the PBNCs/rGO nanocomposite were further characterized by XPS measurements. Both the fully scanned spectra of GO (Fig. 2A) and PBNCs/rGO nanocomposite (Fig. 2B) demonstrate the existence of C and O elements, whereas N1s and Fe2p peaks also appeared in the PBNCs/rGO nanocomposite (Fig. 2B). It is observed that after the reduction, the residual oxygen functionalities were still present on the reduced GO surface. However, the O/C ratio of the reduced GO in the PBNCs/rGO nanocomposite is much lower than that of GO, suggesting considerable deoxygenation during the reduction process. More detailed information on different C bonds of GO and reduced GO is shown in Fig. 2C and D, respectively. Generally, there are four different C groups in GO and reduced GO, including (1) C–C at 284.4 eV, (2) C–O at 286.3 eV, (3) C=O at 287.4 eV, and (4) O–C=O at 288.5 eV. Compared with GO, the reduced GO in the PBNCs/rGO nanocomposite presents a strong suppression of the oxygen-containing components, indicating that GO has been reduced leaving a small number of oxygen functionalities. In addition, there was an additional component at 285.7 eV in Fig. 2D corresponding to the C–N in $[Fe(CN)_6]^{4-}$ and PEI. Furthermore, the main core-level peak of N1s in the PBNCs/rGO nanocomposite can be resolved into three peaks at 397.6, 391.2 and 402.3 eV, as shown in Fig. 2E. We further pay attention to the Fe spectra of the PBNCs/rGO nanocomposite. The binding energies of $Fe2p_{3/2}$ and $Fe2p_{1/2}$ are observed at 712.2 and 721.2 eV, respectively, which are due to the presence of Fe^{3+} (Fig. 2F). The peak at 708.3 eV represents the existence of $Fe2p_{3/2}$ in $[Fe(CN)_6]^{4-}$.[39] All these results demonstrate successful preparation of the PBNCs/rGO nanocomposite.

To investigate the hydrophilicity of the PBNCs/rGO nanocomposite modified electrode, contact angles were measured, as shown in Fig. 3A. One can see that the results of bare electrode and PBNCs/rGO modified electrode are 60.1° and 24.4°, respectively, indicating the fine hydrophilicity of the PBNCs/rGO nanocomposite, which may provide a suitable microenvironment for retaining the activity of biomolecules.[40] In addition, the PBNCs/rGO nanocomposite dispersion is very stable without precipitation for more than 1 month at ambient conditions.

Electrochemical measurements were also used to evaluate the AChE biosensor based on PBNCs/rGO nanocomposite modified SPE (AChE–PBNCs/rGO/SPE). Determination of thiocholine is in fact usually carried out to evaluate the degree of inhibition of AChE and achieve indirect OP pesticides measurements. Fig. 3B compares the cyclic voltammograms of bare electrode and AChE–PBNCs/rGO/SPE in the presence of ATCl. The oxidation of thiocholine, a hydrolysis product of ATCl by AChE, reaches maximum oxidative current at 680 mV obtained at AChE modified SPE (curve a). In the case of AChE–PBNCs/rGO/SPE in PBS buffer, a pair of reversible peaks typifying the oxidation and reduction of PB is clearly observed (curve b). The small distance between peak potentials indicates its adsorption on the electrode surface. When adding 3.0 mM ATCl to the PBS, the oxidation current obtained at AChE–PBNCs/rGO/SPE (curve c) obviously increases compared to that observed in the absence of ATCl (curve b) and the peak potential shifts negatively to 220 mV (curve c). The over-potential decreases ~460 mV compared to curve a, suggesting that PBNCs/rGO has an electrocatalytic activity towards the oxidation of thiocholine. We further studied the amperometric response of ATCl by i–t measurements at the potential of 0.2 V obtained at different AChE modified electrodes including bare SPE, PB/SPE and PBNCs/rGO/SPE, and the results were summarized in Table 1. The oxidation current of thiocholine at bare SPE reached the maximum steady-state current (1.4 μA) with 26 s, while it increased to 10.7 μA at PB/SPE with response time of 20.6 s due to the good electron conductivity of PB and its high electrocatalytic activity. However, when PBNCs/rGO nanocomposite was introduced onto the electrode, further increased current (15.2 μA) and decreased response time (10.9 s) were observed. The results demonstrate that the largest catalytic current is observed at the PBNCs/rGO electrode because of the synergistic effects between the reduced GO and the PB nanocubes on thiocholine oxidation. Other researchers explained the observed synergy by the hypothesis that introducing carbon nanotubes into the polymer matrix containing redox mediators improved its electronic and ionic transport capacity and electron self-exchange in the polymer film.[41,42] This hypothesis can also be applied to our system of a PBNCs/rGO nanocomposite modified electrode. The reduced GO in the nanocomposite improves the electronic and potassium ionic transport capacity, resulting in an enhancement of the electrocatalytic activity. The general reactions on the electrode surface could be as follows:

$$\text{Acetylthiocholine} \xrightarrow{\text{AChE}} \text{Thiocholine} + \text{HA (acetic acid)} \quad (1)$$

$$PB_{ox} + \text{Thiocholine}_{red} \longrightarrow PB_{red} + \text{Thiocholine}_{ox} \quad (2)$$

$$PB_{red} \overset{e^-}{\rightleftharpoons} PB_{ox} \quad (3)$$

The catalytic thiocholine oxidation in the case of PB can be achieved with the redox centre active at ~220 mV, which greatly lowers the oxidation potential for thiocholine detection. The peak current increased and the peak potential shifted slightly with increasing scan rate (data not shown). The peak currents exhibited a linear dependence on the scan rate ranging from 10 to 200 mV s^{-1}, indicating a typical surface-controlled electrode process.

The data from hydrodynamic voltammograms further confirms the electrocatalytic activity of different AChE modified electrodes (Fig. 3C). For comparison, the responses of ATCl on AChE/SPE (curve a), AChE–PB/SPE (curve b), and AChE–PBNCs/rGO/SPE (curve c) under the same conditions are displayed. The bare SPE yields a detectable but small response to thiocholine (curve a). The presence of PB nanoparticles improved the electrocatalytic current due to the mediated redox process of PB (curve b). As expected, the PBNCs/rGO nanocomposite exhibits the highest electrochemical response to thiocholine (curve c), which is consistent with the results of cyclic voltammetric measurement.

The square-wave voltammetric measurement of thiocholine was used for detection of OP pesticides by determining the residual activity of AChE. The decrease in peak current increased with the increase of pesticide concentration. As shown in Fig. 3D, the inhibition efficiency increased with the concentration of monocrotophos from 1.0 to 600 ng mL^{-1}. The detection limit was calculated to be 0.1 ng mL^{-1}, taken as the concentration equivalent to a 10% decrease in signal. It is lower than that of 5 ng mL^{-1}, from the electrodeposited chitosan layer modified AChE biosensor[43] and the AChE/choline oxidase bienzyme amperometric acetylcholine biosensor;[44] and comparable to 0.9 ng mL^{-1} from the 3-mercaptopropionic acid SAM electrode.[45]

The inhibition of AChE by OP pesticides can be reversed by use of nucleophilic compounds such as pralidoxime iodide. With increasing concentration of pralidoxime iodide the reactivation efficiency increased. It is observed that AChE on electrode surface inhibited by monocrotophos can resume 90% of its original activity after immersion in 5.0 mM pralidoxime iodide (Fig. 4A). With increasing reactivation time, the reactivation efficiency increased and reached a constant value after 15 min (Fig. 4B). Based on this reactivation procedure the proposed biosensor could be used repeatedly. The intra-assay precision of the biosensors was evaluated by assaying one enzyme electrode for six replicate determinations in 3.0 mM ATCl. Similarly, the inter-assay precision, or fabrication reproducibility, was estimated at six different electrodes. The RSD of intra-assay and inter-assay were found to be 4.9% and 7.2%, respectively, indicating acceptable reproducibility. When the enzyme electrode was not in use, it was stored at 4 °C in dry conditions. No obvious decrease in the response was observed in the first 10-day storage. After a 30-day storage period, the sensor retained 80% of its initial current response.

To further demonstrate the practicality and accuracy of the proposed biosensor, a series of monocrotophos spiked cucumber samples were used. These samples were prepared by spiking different amounts of monocrotophos with known concentrations to cucumber solution. The results are summarized in Table 2, which shows that the recoveries were in the range of 97–104%, indicating that the proposed electrochemical method is reliable.

Conclusions

In summary, we have developed an AChE biosensor for detection of OPs based on Prussian blue nanocubes/reduced graphene oxide nanocomposite, which was prepared by directly mixing Fe^{3+} and $[Fe(CN)_6]^{3-}$ in the presence of GO in polyethyleneimine aqueous solution. The graphene nanosheet not only acts as a frame to load large amount of cubic PB nanoparticles but also provides a large surface area for large quantities of enzymes to be immobilized. The PBNCs/rGO nanocomposite based AChE biosensor exhibits high electrocatalytic activity towards the oxidation of thiocholine, thus resulting in a rapid response, high sensitivity and low detection potential. The inhibited AChE can be reactivated completely in a short time and therefore the AChE biosensor can be used repeatedly. We are currently working on the disadvantage that the inhibition based AChE biosensor is not specific to particular kinds of organophosphate and carbamate pesticides. However, this does not necessarily compromise its value based on this mode. The ease of performance and the cost effectiveness of the proposed AChE biosensor have a great potential for application in on-site detection of the total amount of pesticides.

Acknowledgements

This work was supported by the National Natural Science Foundation of China (21075047, 21172087) and self-determined research funds of CCNU from the colleges' basic research and operation of MOE (CCNU11C01002, CCNU10A02005). Y. Lin acknowledges the financial support by Grant U54 ES16015 from the National Institute of Environmental Health Sciences, the National Institute of Health (NIH) and a LDRD program funded by the U.S. Department of Energy (DOE). The contents of this publication are solely the responsibility of the authors and do not necessarily represent the official views of the NIH. Pacific Northwest National Laboratory is operated by Battelle for US-DOE under Contract DE-AC05-76RL01830. We specially thank Prof. Ruikang Tang in Zhejiang University for characterization of the nanocomposite.

Notes and references

1 M. Jokanović and M. Kosanović, *Environ. Toxicol. Pharmacol.*, 2010, **29**, 195–201.
2 J. E. Casida, *J. Agric. Food Chem.*, 2011, **59**, 2762–2769.
3 N. Fidalgo-Used, E. Blanco-González and A. Sanz-Medel, *Talanta*, 2006, **70**, 1057–1063.
4 K. D. Lin, S. S. Zhou, C. Xu and W. P. Liu, *J. Agric. Food Chem.*, 2006, **54**, 8134–8138.
5 D. Du, W. J. Chen, W. Y. Zhang, D. L. Liu, H. B. Li and Y. H. Lin, *Biosens. Bioelectron.*, 2010, **25**, 1370–1375.
6 (*a*) D. Du, X. X. Ye, J. Cai, J. Liu and A. D. Zhang, *Biosens. Bioelectron.*, 2010, **25**, 2503–2508; (*b*) D. Du, S. Z. Chen, D. D. Song, H. B. Li and X. Chen, *Biosens. Bioelectron.*, 2008, **24**, 475–479; (*c*) D. Du, S. Z. Chen, J. Cai and D. D. Song, *J. Electroanal. Chem.*, 2007, **611**, 60–66.
7 G. D. Liu and Y. H. Lin, *Anal. Chem.*, 2006, **78**, 835; G. D. Liu, S. L. Riechers, M. C. Mellen and Y. H. Lin, *Electrochem. Commun.*, 2005, **7**, 1163–1169.
8 J. L. Marty, N. Mionetto, F. Ortega and C. Roux, *Biosens. Bioelectron.*, 1993, **8**, 273–280.
9 J. L. Marty, N. Mionetto, S. Lacorte and D. Barceló, *Anal. Chim. Acta*, 1995, **311**, 265–271.
10 J. P. Hart and I. C. Hartley, *Analyst*, 1994, **119**, 259–263.

11 W. A. Collier, M. Clear and A. L. Hart, *Biosens. Bioelectron.*, 2002, **17**, 815–819.
12 F. Ricci, F. Arduini, A. Amine, D. Moscone and G. Palleschi, *J. Electroanal. Chem.*, 2004, **563**, 229–237.
13 H. D. Chen, X. L. Zuo, S. Su, Z. Z. Tang, A. B. Wu, S. P. Song, D. B. Zhang and C. H. Fan, *Analyst*, 2008, **133**, 1182–1186.
14 K. S. Novoselov, A. K. Geim, S. V. Morozov, D. Jiang, Y. Zhang, S. V. Dubonos, I. V. Grigorieva and A. A. Firsov, *Science*, 2004, **306**, 666–669.
15 A. K. Geim and K. S. Novoselov, *Nat. Mater.*, 2007, **6**, 183–191.
16 A. H. Castro Neto, F. Guinea, N. M. R. Peres, K. S. Novoselov and A. K. Geim, *Rev. Mod. Phys.*, 2009, **81**, 109–162.
17 L. H. Tang, Y. Wang, Y. Liu and J. H. Li, *ACS Nano*, 2011, **5**, 3817–3822.
18 S. J. Guo and S. J. Dong, *J. Mater. Chem.*, 2011, **21**, 16704–16716.
19 Y. Y. Shao, J. Wang, H. Wu, J. Liu, I. A. Aksay and Y. H. Lin, *Electroanalysis*, 2010, **22**, 1027–1036.
20 Y. X. Fang, S. J. Guo, C. Z. Zhu, Y. M. Zhai and E. K. Wang, *Langmuir*, 2010, **26**, 11277–11282.
21 S. Zhang, Y. Y. Shao, H. G. Liao, J. Liu, I. A. Aksay, G. P. Yin and Y. H. Lin, *Chem. Mater.*, 2011, **23**, 1079–1081.
22 Y. C. Qiu, K. Y. Yan, S. H. Yang, L. M. Jin, H. Deng and W. S. Li, *ACS Nano*, 2010, **4**, 6515–6526.
23 O. Akhavan, M. Abdolahad, A. Esfandiar and M. Mohatashamifar, *J. Phys. Chem. C*, 2010, **114**, 12955–12959.
24 S. M. Paek, E. J. Yoo and I. Honma, *Nano Lett.*, 2009, **9**, 72–75.
25 C. Nethravathi, J. T. Rajamathi, N. Ravishankar, C. Shivakumara and M. Rajamathi, *Langmuir*, 2008, **24**, 8240–8246.
26 M. Seredych and T. J. Bandosz, *Carbon*, 2007, **45**, 2130–2132.
27 Z. Liu, J. Robinson, X. M. Sun and H. J. Dai, *J. Am. Chem. Soc.*, 2008, **130**, 10876–10877.
28 X. Y. Yang, X. Y. Zhang, Y. F. Ma, Y. Huang, Y. S. Wang and Y. S. Chen, *J. Mater. Chem.*, 2009, **19**, 2710–2714.
29 S. Watcharotone, D. A. Dikin, S. Stankovich, R. Piner, I. Jung, G. H. B. Dommett, G. Evmenenko, S. E. Wu, S. F. Chen, C. P. Liu, S. T. Nguyen and R. S. Ruoff, *Nano Lett.*, 2007, **7**, 1888–1892.
30 H. Bai, Y. X. Xu, L. Zhao, C. Li and G. Q. Shi, *Chem. Commun.*, 2009, 1667–1669.
31 G. H. Lu, S. Mao, S. J. Park, R. S. Ruoff and J. H. Chen, *Nano Res.*, 2009, **2**, 192–200.
32 X. Z. Zhou, X. Huang, X. Y. Qi, S. X. Wu, C. Xue, F. Y. C. Boey, Q. Y. Yan, P. Chen and H. Zhang, *J. Phys. Chem. C*, 2009, **113**, 10842–10846.
33 C. Xu, X. Wang, J. W. Zhu, X. J. Yang and L. D. Lu, *J. Mater. Chem.*, 2008, **18**, 5625–5629.
34 X. M. Chen, G. H. Wu, J. M. Chen, X. Chen, Z. X. Xie and X. R. Wang, *J. Am. Chem. Soc.*, 2011, **133**, 3693–3695.
35 E. Jin, X. F. Lu, L. L. Cui, D. M. Chao and C. Wang, *Electrochim. Acta*, 2010, **55**, 7230–7234.
36 X. W. Liu, Z. J. Yao, Y. F. Wang and X. W. Wei, *Colloids Surf., B*, 2010, **81**, 508–512.
37 E. Suprun, G. Evtugyn, H. Budnikov, F. Ricci, D. Moscone and G. Palleschi, *Anal. Bioanal. Chem.*, 2005, **383**, 597–604.
38 L. Y. Cao, Y. L. Liu, B. H. Zhang and L. H. Lu, *ACS Appl. Mater. Interfaces*, 2010, **2**, 2339–2346.
39 K. B. Yatsimirskii, V. V. Nemoshkalenko, Y. P. Nazarenko, V. G. Aleshin, V. V. Zhilinskaya and N. A. Tomashevsky, *J. Electron Spectrosc. Relat. Phenom.*, 1977, **10**, 239–245.
40 H. Kaji, M. Kanada, D. Oyamatsu, T. Matsue and M. Nishizawa, *Langmuir*, 2004, **20**, 16–19.
41 M. G. Zhang and W. Gorski, *J. Am. Chem. Soc.*, 2005, **127**, 2058–2059.
42 M. G. Zhang and W. Gorski, *Anal. Chem.*, 2005, **77**, 3960–3965.
43 D. Du, X. Huang, J. Cai, A. D. Zhang, J. W. Ding and S. Z. Chen, *Anal. Bioanal. Chem.*, 2006, **387**, 1059–1065.
44 S. Hou, Z. Ou, Q. Chen and B. Wu, *Biosens. Bioelectron.*, 2012, **33**, 44–49.
45 V. A. Pedrosa, J. Caetano, S. A. S. Machado, R. S. Freire and M. Bertottia, *Electroanalysis*, 2007, **19**, 1415–1420.